Postprint of: Zych M., Hanus R., Wilk B., Petryka L., Świsulski D., Comparison of noise reduction methods in radiometric correlation measurements of two-phase liquid-gas flows, Measurement, Vol. 129 (2018), pp. 288-295, DOI: 10.1016/j.measurement.2018.07.035

Comparison of noise reduction methods in radiometric correlation measurements of two-phase liquid-gas flows

Marcin Zych [a1], Robert Hanus [b], Barbara Wilk [b], Leszek Petryka [c], Dariusz Świsulski [d]

[a] AGH University of Science and Technology, Faculty of Geology, Geophysics and Environmental Protection, Al. Mickiewicza 30, 30-059 Kraków, Poland
[b] Rzeszów University of Technology, Faculty of Electrical and Computer Engineering, Powstanców Warszawy 12, 35-959 Rzeszów, Poland
[c] AGH University of Science and Technology, Faculty of Physics and Applied Computer Science, Al. Mickiewicza 30, 30-059 Kraków, Poland
[d] Gdańsk University of Technology, Faculty of Electrical and Control Engineering, 80-233 Gdańsk, Poland

Abstract: Two-phase liquid-gas flows occur frequently in the mining, energy, chemical, and petrochemical industries. One of non-contact methods used to analyse these flows is the gamma ray absorption method. However, the signals received from radiation detectors contain a significant stochastic noise, which makes them difficult to analyse. The article describes four methods of noise reduction in cross-correlation measurements of water-air mixture flows in a horizontal pipeline. In addition to the classical method of digital filtering of signals, the methods consisting in signal spectrum filtering, discrete wavelet transformation, and Nadaraya-Watson kernel estimator are described. Sample results of the measurements carried out in the horizontal pipe having the inner diameter of 30 mm for the air bubbles velocity ranging from 0.7 to 1.4 m/s are presented. In the research, the absorption set composed of two linear Am-241 gamma-ray sources and two scintillation NaI(Tl) probes was used. It was found that the lowest measurement uncertainty of the dispersed phase flow velocity is obtained when the cross-correlation

[1] Corresponding author. E-mail: zych@geol.agh.edu.pl; phone:+48 12 617 23 53, fax: +48 12 633 29 36

distributions of the recorded signals are smoothed using the Discrete Wavelet Transform or the Nadaraya-Watson kernel estimator.

Keywords: two-phase flow, gamma ray absorption, cross-correlation, cross-spectral density, Discrete Wavelet Transform, Nadaraya-Watson kernel estimator

1. Introduction

Two-phase liquid-gas flows can be observed in mining, chemical, petrochemical, food, and energy industries. Measuring parameters of such flows, for example the velocities of individual phases and their involvement in the mixture, etc., is not simple and requires sophisticated and often non-invasive measurement techniques. In recent years, methods using capacitive, resistive, optical, or X-ray tomography have been developed [1-5]. Other techniques are: particle image velocimetry (PIV), speed camera, and ultrasonic or Coriolis flowmeters [6-11]. For many years, two-phase flows have also been studied by radioisotopes [12-15].

For the liquid-gas flow, the mean velocity of the dispersed phase can be calculated on the basis of its transportation time delay recognized between two signals obtained from the scintillation probes. After specific pre-processing, these signals become ergodic, so due to the stochastic nature of radiation, they can be analysed in time and frequency domains. The methods to be applied in this case may include such functions as: differential or combined cross-correlation (*CCF*), *CCF* with Hilbert transform, conditional averaging, deconvolution, and the phase method [16-23]. However, the signals received directly from the probes are often inconvenient for analysing due to the presence of significant noise (background radiation, nuclear decay fluctuations, noise generated by the electronics, etc.) [23,24]. Often, the level of disturbances is so high

that the most commonly used cross-correlation method does not always give accurate results. Therefore, the noise level in the recorded signals is to be reduced before calculating the CCF. Alternatively, smoothing of the CCF can be applied. The use of advanced noise reduction methods can give a more accurate determination of the dispersed phase transportation time delay and then its velocity, as well as other parameters of the flow. The considered procedure is also of high importance in other fields of science and technology, e.g. in geophysics, or medicine [25-30].

The article describes the application of selected noise reduction methods in cross-correlation measurements, with the liquid-gas mixture flow in a horizontal pipeline as an example. In addition to classical digital filtering of recorded signals, three other methods: the method based on "spectrum filtering", the discrete wavelet transform, and the Nadaraya-Watson kernel estimator, are applied [31-39]. Section 2 gives the description of the experimental setup used for conducting the study. Section 3 presents the idea of the radioisotope method and the absorption set used for the measurement. In Section 4, the basic information about the time delay estimation using cross-correlation techniques is overviewed, while Section 5 describes the noise reduction methods used in the article. Section 6 summarizes the obtained results, and the final section presents conclusions drawn from the research.

2. Experimental setup

The analysis presented in the article makes use of the results of experiments performed on an experimental setup built at the AGH University of Science and Technology in Krakow, Poland, the Faculty of Physics and Applied Computer Science

[16,20,23]. The main part of the setup is a hydraulic installation the diagram of which is shown in Fig. 1. The installation consists of a horizontal pipeline made of Plexiglas with length of 4.5 m and inner diameter of 30 mm. It is connected via a hose to a rotary pump (4), which forces the water circulation. The expansion tank (6) acts also as a venting system. To produce the mixture, the required air volume is forced into the pipeline from the compressor (5) via the nozzle (7). The absorption measuring set consists of the radioactive sources in collimators (1) and two scintillation probes (2). The set is mounted in a sliding arrangement (8) to allow the equipment to move along the pipe. The geometry of the deployed absorption set is described in detail in Section 3. A complementary element to the radiometric system is the ultrasonic meter Uniflow 990 (3) which measures the water flow rate.

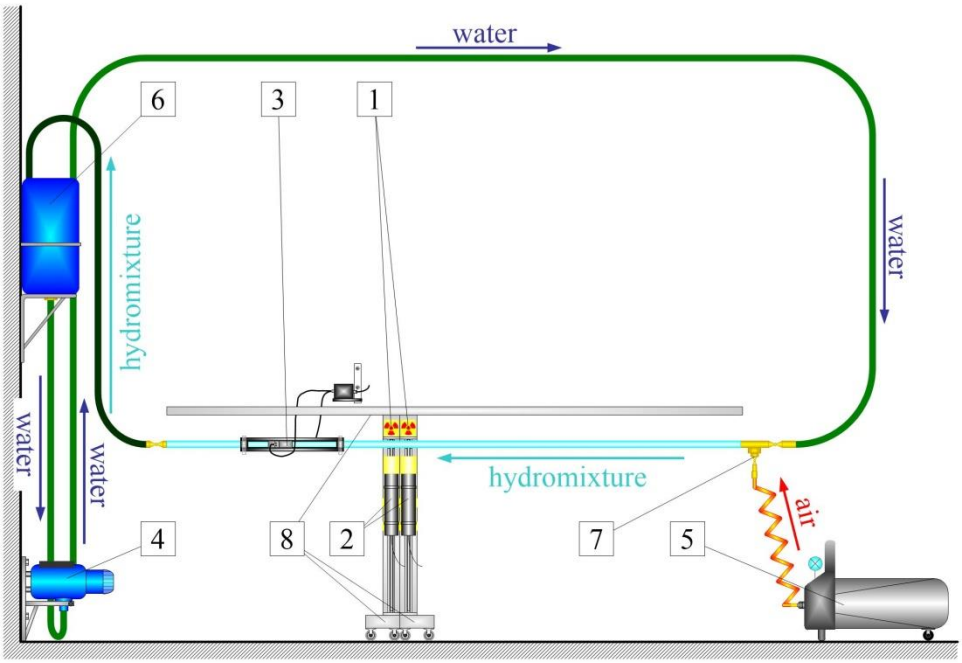

Fig. 1. Diagram of installation used for liquid-gas mixture flow tests: 1 - lead collimators of gamma radioactive sources, 2 - scintillation probes, 3 - ultrasonic flowmeter, 4 – rotary pump, 5 - air compressor, 6 - expansion tank, 7 - air nozzle, 8 - shifter kit of the absorption set [16].

Adjusting the pump speed within the range between 1000 and 2800 rpm allows to generate various flow patterns in the measuring section of the pipeline. Three characteristic flow structures selected for analysing in the paper are shown in Fig. 2.

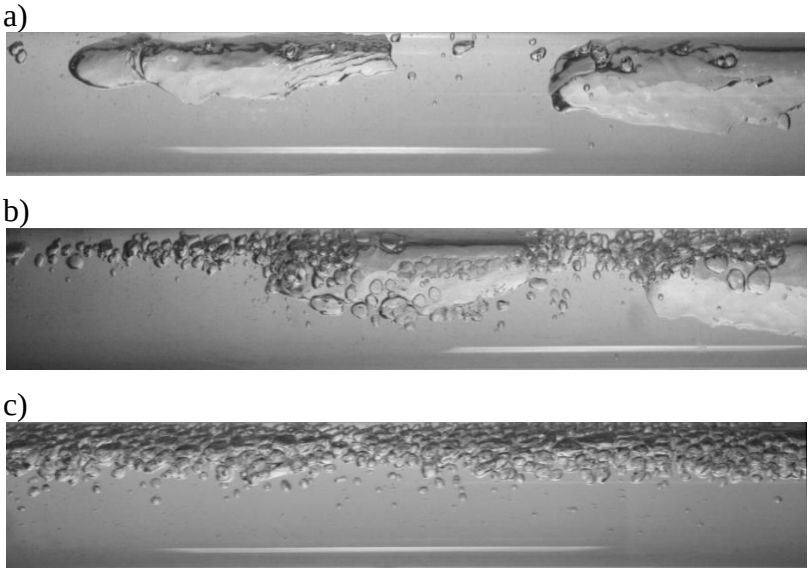

Fig. 2. Flow patterns selected for analysing : a) plug flow, b) transitional plug – bubble flow, c) bubble flow.

3. Measuring technique of gamma-ray absorption

In the hydraulic installation, an absorption set composed of two gamma-ray sources and two probes spaced by the distance $L = 97$ mm was applied. The principle of the gamma absorption measurement and the geometry of the absorption set are shown in Fig. 3.

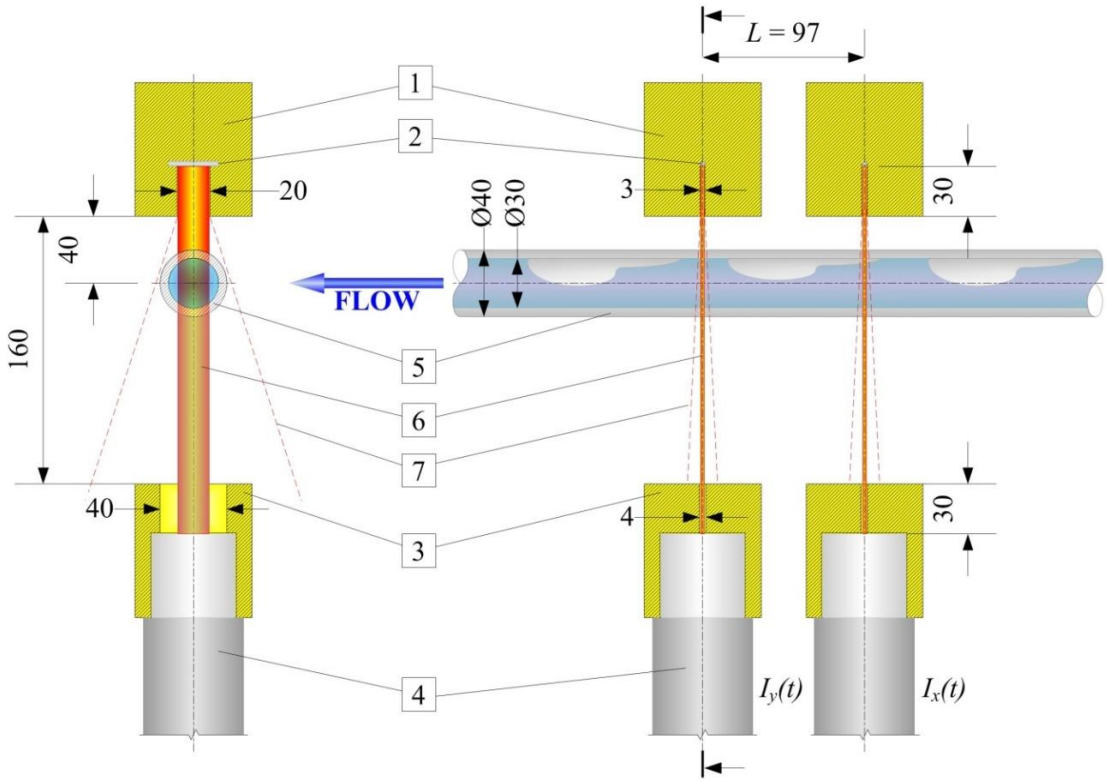

Fig. 3. Principle and geometry of the gamma absorption measurement: 1 - lead collimators shaping gamma-ray beams, 2 - linear radioactive sources, 3 – detectors' collimators eliminating scattered radiation, 4 - scintillation probes, 5 - pipeline with the two-phase mixture, 6 - main beam of gamma rays, 7 - distributed beam of gamma radiation. All dimensions given in mm [16].

The gamma radiation beam (5) emitted by the source shaped in the lead collimators (1) passes through the pipe with the flowing liquid-gas mixture (4). As a result of the impact of gamma rays on atoms of the flowing mixture, a weakened beam reaches the scintillation probes (2) mounted in collimators (3) which protect the detectors against scattered and dispersed radiation (7). The measurement geometry allows for registering radiation force changes in a given pipe cross section. The slots in source collimators are 3 mm wide and 20 mm long, while those in detector collimators have dimensions of 4 mm and 40 mm, respectively. Based on earlier gained experience and performed calculations, the geometry of the measurement system was established in such a way as

to ensure the most optimal measurement environment (precise X-ray of the given section with the gamma radiation beam).

For the measurements, the linear radioactive sources Am-241 X.103 AEA Technology QSA, emitting the energy of 59.5 keV and 100 mCi activity, and the probes with scintillation crystals NaI(Tl) type SKG-1, TESLA Company were used.

The gamma radiation intensity changes caused by the water-air mixture flowing through the measuring pipe section give the signals $I_x(t)$ and $I_y(t)$ at outputs of the scintillation probes (Fig. 4 a, b).

a) b)

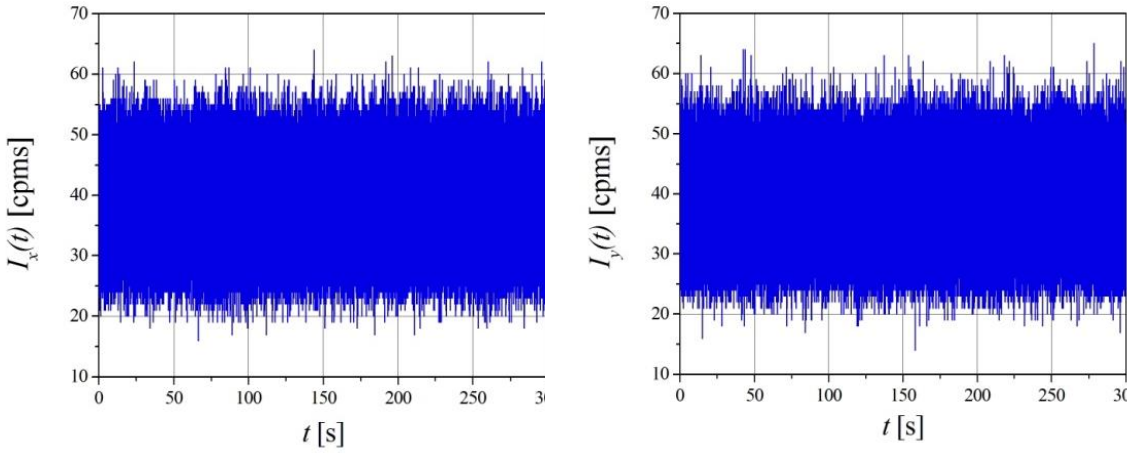

Fig. 4**.** Scintillation probe signals recorded in BUB004 experiment.

In each experiment, the signals were sampled uniformly after time $\Delta t = 1$ ms and recorded within the time interval of 300 s. This resulted in their digital representation having the form of functions $x(n)$ and $y(n)$, where $n = t/\Delta t$.

4. Time delay estimation by cross-correlation

The signals from scintillation probes can be used to determine the transportation time delay τ_0. The best-known classical method of time delay estimation of an ergodic random signal is based on the cross-correlation function defined as follow [17,18]:

$$R_{xy}(\tau) = \lim_{T\to\infty} \frac{1}{T} \int_0^T x(t)y(t+\tau)dt \tag{1}$$

where T is the averaging time and τ is the time delay.

The transportation time delay τ_0 is determined based on the *CCF* maximum position:

$$\hat{\tau}_0 = \arg\left\{\max R_{xy}(\tau)\right\} = \arg\left\{R_{xy}(\tau_0)\right\} \tag{2}$$

The discrete estimator for the cross-correlation function can be expressed by the following formula:

$$R_{xy}(\tau) = \frac{1}{N} \sum_{n=0}^{N-1} x(n)y(n+\tau) \tag{3}$$

where N is the number of values of discrete signals $x(n)$ and $y(n)$.

For large data sets, the *CCF* is calculated using the *DFT/FFT*.

Once the estimation of the transportation time delay and the distance L between the probes are known, the average gas phase velocity υ can be calculated from the formula:

$$\upsilon = L / \hat{\tau}_0 \tag{4}$$

The experimental setup described in Section 2 was used for a number of experiments with various parameters of the water-air flow.

In selected experiments with air volume concentration in the flow equal to 0.3, increasing the water velocity υ_W led to different forms of flow, as shown in Fig. 2:

- experiment BUB006: υ_W = 0.90 m/s – plug flow,

- experiment BUB004: υ_W = 1.36 m/s – transitional plug – bubble flow,

- experiment BUB001: υ_W = 1.92 m/s – bubble flow.

Fig. 5 shows the *CCF* charts designated for the signals received from the scintillation probes in experiments BUB006, BUB004 and BUB001. Raw signals were used in these cases, and that is why the location of the *CCF* maximum is difficult to ascertain due to the presence of noise. This is particularly evident in the BUB001experiment (Fig. 5c).

a) b) c)

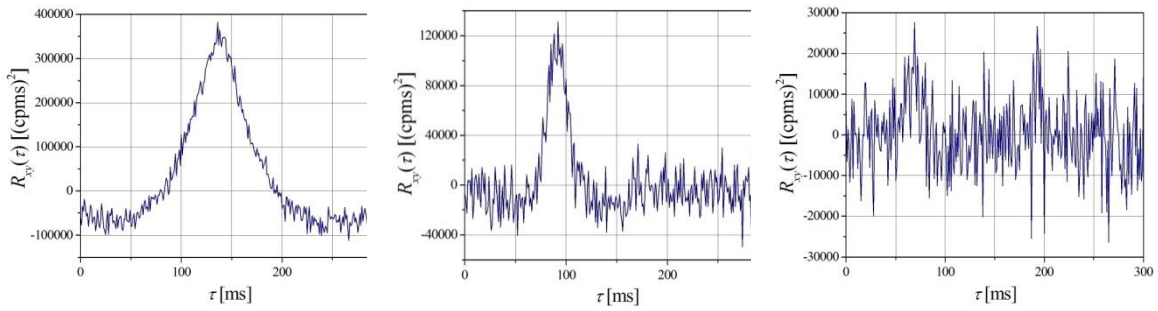

Fig. 5. *CCF* determined in experiments: a) BUB006, b) BUB004, c) BUB001.

5. Selected noise reduction methods

There are several noise reduction methods which can be applied in radioisotope measurements of two-phase flows with the use of correlation calculations. This section describes the noise reduction performed directly in the measuring signals, prior to the correlation analysis (classical digital filtering and "spectrum filtration"), as well as smoothing the raw *CCF* using the discrete wavelet transform and the Nadaraya-Watson kernel estimator.

5.1.Classical digital filtering

Since the signals obtained from the scintillation probes are discrete, we can directly apply the classical digital filters to reduce the noise. The results obtained with the use of the classical Infinite Impulse Response (*IIR*) Butterworth fourth-order band-pass filter are presented.

The general difference equation (5) which characterizes *IIR* filters is:

$$y_i = \sum_{j=0}^{N_b-1} b_j x_{i-j} - \sum_{k=1}^{N_a-1} a_k y_{i-k} \tag{5}$$

where b_j is the set of forward coefficients, N_b is the number of forward coefficients, a_k is the set of reverse coefficients, N_a is the number of reverse coefficients, x_i is the current input, x_{i-j} is the past j-th input, and y_{i-k} is the past k-th output.

Consequently, the filter passbands f_{BP} were chosen individually for the registered signals. The signals processed in this way were used to calculate the cross-correlation function from the formula (3). Fig. 6 shows the *CCF* graphs obtained in experiments BUB006, BUB004 and BUB001. The dashed line represents the position of the *CCF* maximum which indicates the estimated average transportation time delay of gas phase.

a) b) c)

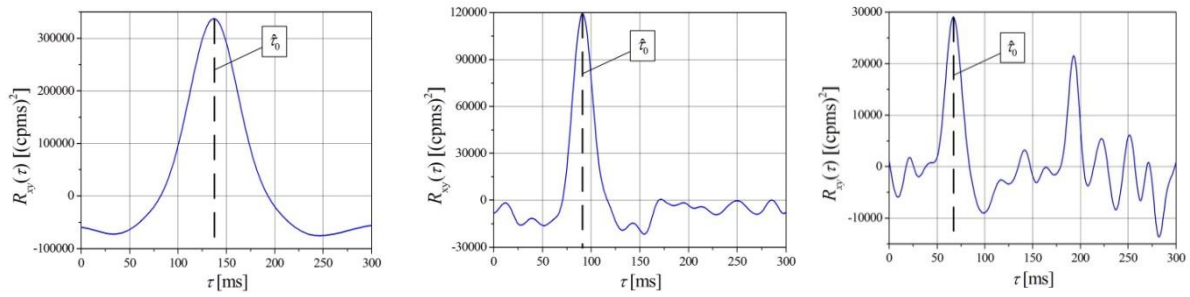

Fig. 6. *CCF* improvement after classical digital filtration of recorded signals in experiments: a) BUB006 (f_{BP} = 0.1 – 17.0 Hz), b) BUB004 (f_{BP} = 0.1 – 45.0 Hz), c) BUB001 (f_{BP} = 0.1 – 50.0 Hz).

5.2.Frequency band processing

The analyses conducted by the authors have shown how proper estimation of the time delay by the *CCF* method can be obtained and how using the "spectrum filtration" facilitates this process. The above operation consists in determining the cross-spectral density of the signal and then cutting off all frequencies falling outside of the chosen useful bandwidth. The inverse *DFT* of the so-obtained spectrum gives the useful cross-correlation distribution. The useful frequency range f_u can be selected based on the auto spectral density function (*ADF*), or the module of the cross-spectral density function (*CSDF*) of signals $x(n)$ and $y(n)$. The values of *ADF* $G_{xx}(f)$ and *CSDF* $\underline{G}_{xy}(f)$, derived in practice for frequency range $0 < f < \infty$, can be given by equations:

$$G_{xx}(f) = 2\int_{-\infty}^{\infty} R_{xx}(\tau) e^{-j2\pi f\tau} d\tau \tag{6}$$

$$\underline{G}_{xy}(f) = 2\int_{-\infty}^{\infty} R_{xy}(\tau) e^{-j2\pi f\tau} d\tau \tag{7}$$

where $R_{xx}(\tau)$ is the autocorrelation function of signal $x(t)$.

The experiments carried out by the authors have also shown that the improvement of the results can be obtained by using the *CSDF* procedure [16]. Unfortunately, due to large variance of raw (unsmoothed) *ADF* and *CSDF* values, determining the useful frequency range is difficult.

The authors propose that the useful frequency range f_u is determined with the use of the *CSDF* module $|\underline{G}_{xy}(f)|$:

$$\left|\underline{G}_{xy}(f)\right| = \left\{\mathrm{Re}\left[\underline{G}_{xy}(f)\right]^2 + \mathrm{Im}\left[\underline{G}_{xy}(f)\right]^2\right\}^{0,5} \tag{8}$$

after prior frequency smoothing [19].

The frequency smoothed estimator $|\underline{G}_{xy}(f)|_s$ is defined by the equation:

$$\left|\underline{G}_{xy}(f_i)\right|_s = \frac{1}{h}\sum_{j=1}^{h}\left|\underline{G}_{xy}(f_{i+j})\right| \tag{9}$$

where h is the length of the smoothing window.

The smoothed *CSDF* module $|\underline{G}_{xy}(f)|_s$ is shown in Fig. 7 d, e and f. The width of the applied smoothing window was h = 400 samples. For comparison, Fig. 7 a, b and c show $G_{xx}(f)_s$ smoothed in the exact same way. It is straightforward to note that for measurements BUB004 and BUB001 it is much easier to determine the useful range of frequencies f_u based on $|\underline{G}_{xy}(f)|_s$. The respective ranges of frequencies f_u are indicated with frames in Fig. 7 d, e and f.

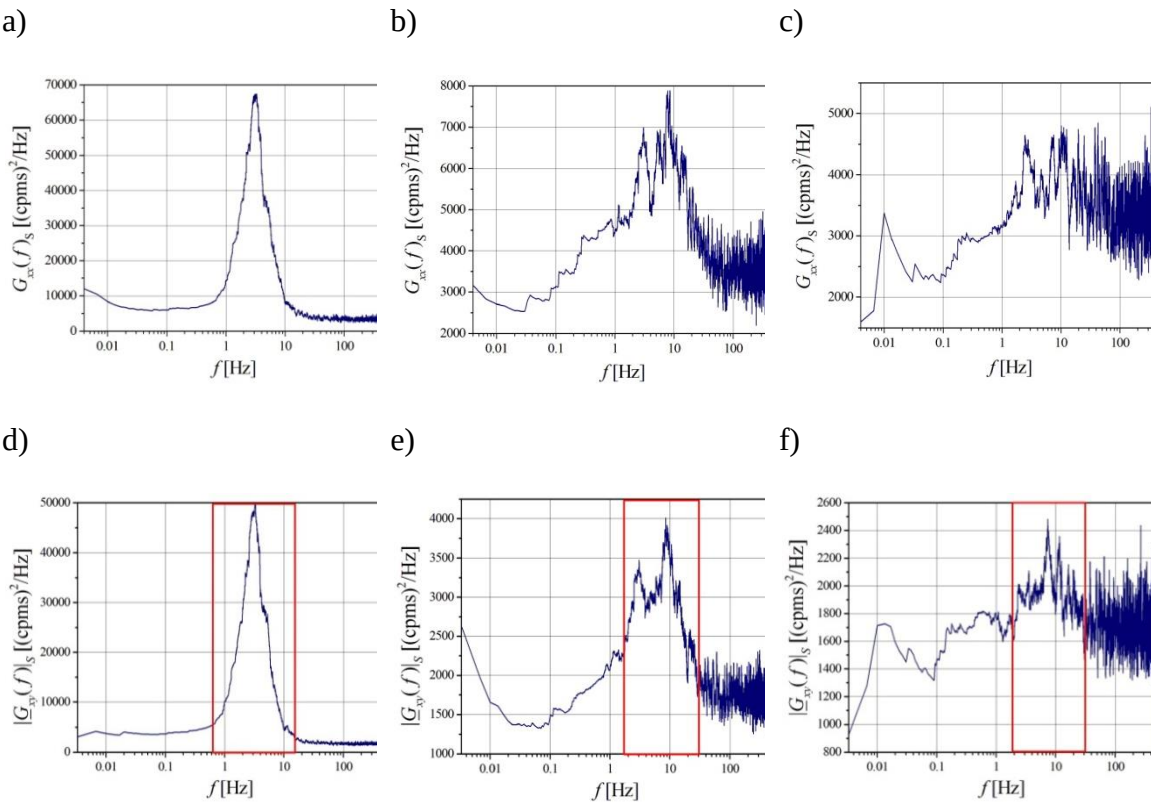

Fig. 7. $G_{xx}(f)_s$ and $|\underline{G}_{xy}(f)|_s$ distributions smoothed with window of h = 400 samples, for signals recorded in experiments: a) and d) BUB006; b) and e) BUB004; c) and f) BUB001. The red frame indicates the useful frequency range f_u.

Fig. 8 shows the cross-correlation function graphs obtained after the completion of the above described „ spectrum filtering" for $|\underline{G}_{xy}(f)|_s$.

a) b) c)

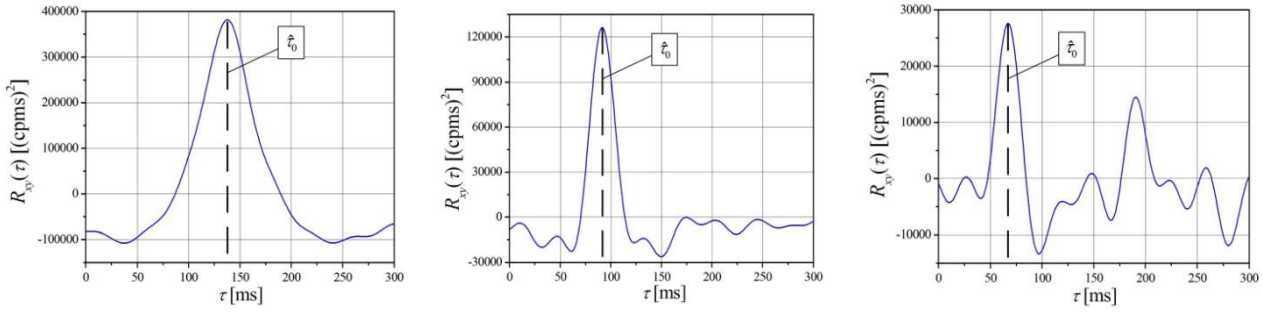

Fig. 8. *CCF* distributions obtained using $|CSDF|_s$: a) BUB006 (f_u = 1.7 – 26.7 Hz), b) BUB004 (f_u = 0.9 – 28.7 Hz), c) BUB001 (f_u = 2.0 – 30.0 Hz).

5.3. CCF smoothing with wavelet transform

On the basis of Fig. 5 we can conclude that the cross-correlation function has an extremely low frequency component, which represents the *CCF* without interference (denoised *CCF*), and a component of higher frequency, which represents the undesired noise. These components can be separated using the wavelet transform.

The core of the wavelet transformation is the base function $\psi(t) \in L^2(R)$, the so-called wavelet base, which must comply with certain conditions [34]. A family of base functions can be created from the basic wavelet (i.e. the mother wavelet) by scaling and time offsetting:

$$\psi_{a,b}(t) = \frac{1}{\sqrt{|a|}}\psi\left(\frac{t-b}{a}\right), \quad a,b \in R, \; a \neq 0, \tag{10}$$

where a is the scale (i.e. expansion rate), and b is the shift in the time domain.

The wavelet transformation allows to obtain the representation of the non-stationary signal in the time-scale by means of the so-called wavelet coefficients that reflect the degree of correlation between the signal and the wavelet $\psi_{a,b}(t)$ for varying parameters a and b. The delay determines the position of the wavelet $\psi_{a,b}(t)$, and the parameter a determines its frequency properties ($a \sim 1/f$). The wavelet transformation can be considered as an analysis conducted using a mid-capacity filter bank characterized by constant goodness (defined as the bandwidth-to-centre-frequency ratio of the filter).

Discrete Wavelet Transform (*DWT*) is defined only for the values of the parameters $a = 2^j$, $b = 2^j k$ ($j, k \in \mathrm{Z}$). The wavelets used for the analysis have a so-called scaling function which can be written as:

$$\begin{aligned} \psi_{j,k}(t) &= 2^{\frac{-j}{2}} \psi(2^{-j}t - k) \\ \varphi_{j,k}(t) &= 2^{\frac{-j}{2}} \varphi(2^{-j}t - k) \end{aligned} \tag{11}$$

Such a wavelet family creates an orthonormal basis in the space $L^2(R)$. To determine *DWT*, we can use an iterative Mallat algorithm [35,36], i.e. the simple and fast algorithm which decomposes the analysed signal to the low-frequency components (so-called approximations A) and the high-frequency component (i.e. detail D) using a digital filter based on the formula:

$$\begin{aligned} \psi(t) &= \sqrt{2} \cdot \sum_{k \in Z} g_k \varphi(2t - k) \\ \varphi(t) &= \sqrt{2} \cdot \sum_{k \in Z} h_k \varphi(2t - k) \end{aligned} \tag{12}$$

where the coefficients g_k and h_k represent the high-pass filter and the low-pass filter, respectively.

The multiresolution decomposition of the *CCF* signal by the Mallat algorithm was conducted using the wavelet "db10". In general, Daubechies constructs orthonormal wavelets with compact support with the maximum number of vanishing moments. The maximum number of zero moments of the wavelets results in a high degree of smoothness for the scaling and wavelet functions. It was determined experimentally that the fifth low-frequency component (i.e. approximation A5) accurately approximates the non-linear, low-frequency component of the *CCF* signal, while the details (i.e. high-frequency D1 to D5) represent only interference. During signal reconstruction, all details were omitted, i.e. only the approximation A5 was used.

The effect of this *CCF* processing is shown in Fig. 9. The dashed line represents the position of the maximum of *CCF*, which indicates the estimated average delay time of the transport.

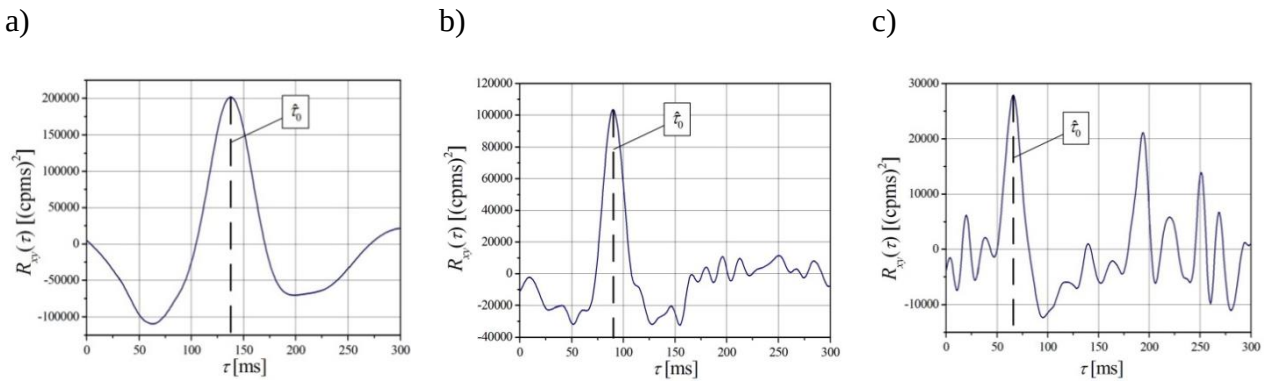

Fig. 9. CCF_S after smoothing with *DWT* (db 10) for experiments: a) BUB006, b) BUB004, c) BUB001.

5.4. CCF smoothing with Nadaraya-Watson kernel estimator

The Nadaraya-Watson kernel estimator (*NWKE*) is a non-parametric regression method. The algorithm allows to introduce the weights $w_{n,i}$ for values τ_i depending on the distance of the point τ which is the centre of the neighbourhood. The *NWKE* is determined as follows [31,32,37]:

$$\hat{g}_{NW}(\tau) = \sum_{i=1}^{n} w_{n,i} R_{xyi} \,, \tag{13}$$

and $w_{n,i}$ is expressed as:

$$w_{n,i}(\tau) = \frac{K\left((\tau - \tau_i)/h_n\right)}{\sum_{j=1}^{n} K\left((\tau - \tau_i)/h_n\right)}, \tag{14}$$

where $K((\tau - \tau_i)/h_n)$ is the kernel function, e.g. the Epanechnikov function, normal or triangular distribution, and h_n is the smoothing bandwidth. In the presented calculations, normal distribution was used.

The parameter h_n can be selected by the user, e.g. through optimization, such as the cross-validation method. The application of the *NWKE* for *CCF* is shown in Fig. 10. The dashed line represents the position of the maximum of *CCF*, which indicates the estimated average delay time of the transport.

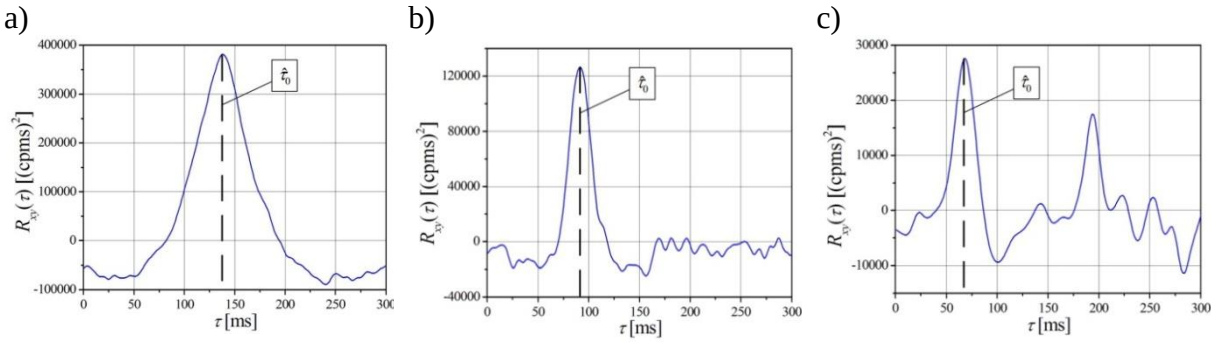

Fig. 10. *CCF* from Fig. 5 after *NWKE* based noise reduction for experiments: a) BUB006 (h_n = 3), b) BUB004 (h_n = 3), c) BUB001 (h_n = 6).

6. Results

In order to estimate the transportation time delay $\hat{\tau}_0$ and its standard uncertainty $u_A(\hat{\tau}_0)$, an interpolation was used for *CCF* as a normal distribution function [23], as shown in Figs. 6, 8, 9 and 10. Then, the transportation time delay standard uncertainty

$u_A(\hat{\tau}_0)$ and the relative standard uncertainty $u_{Ar}(\hat{\tau}_0)$ were determined from the relationships:

$$u_A(\hat{\tau}_0) = \frac{\sigma}{\sqrt{k}} \tag{15}$$

$$u_{Ar}(\hat{\tau}_0) = \frac{u_A(\hat{\tau}_0)}{\hat{\tau}_0} \cdot 100\% \tag{16}$$

where σ is the standard deviation of the fitted Gaussian distribution, and *k* is the number of points used for interpolation.

The time delay estimation results and the uncertainties are given in Table 1.

Tab. 1. Transportation time delay values and uncertainties.

Experiment / Noise filtering method	BUB006			BUB004			BUB001		
	$\hat{\tau}_0$ [ms]	$u_A(\hat{\tau}_0)$ [ms]	$u_{Ar}(\hat{\tau}_0)$ [%]	$\hat{\tau}_0$ [ms]	$u_A(\hat{\tau}_0)$ [ms]	$u_{Ar}(\hat{\tau}_0)$ [%]	$\hat{\tau}_0$ [ms]	$u_A(\hat{\tau}_0)$ [ms]	$u_{Ar}(\hat{\tau}_0)$ [%]
IIR filters	137.0	2.4	1.8	91.2	1.8	2.0	67.0	1.6	2.4
$\lvert CSDF \rvert_s$	136.6	2.1	1.5	91.0	1.5	1.7	66.3	1.4	2.1
DWT	136.2	1.8	1.3	90.7	1.3	1.4	66.3	1.1	1.7
NWKE	136.7	1.9	1.4	90.7	1.4	1.5	66.3	1.3	2.0

The average velocity of the gas phase υ was calculated from Equation (4). Following the law of propagation of uncertainty, the combined standard uncertainty $u_C(\upsilon)$ of the gas phase flow velocity can be determined from the formula [40]:

$$u_C(\upsilon) = \sqrt{\left[\frac{\partial \upsilon}{\partial L} u_B(L)\right]^2 + \left[\frac{\partial \upsilon}{\partial \hat{\tau}_0} u_A(\hat{\tau}_0)\right]^2} \tag{17}$$

where $u_B(L)$ = 0.1 mm is the standard uncertainty of measurement at the distance L.

Indexes A and B are the uncertainties of type A and B, respectively.

The relative combined standard uncertainty $u_{Cr}(\upsilon)$ was calculated from equation:

$$u_{Cr}(\upsilon) = \frac{u_C(\upsilon)}{\upsilon} \cdot 100\% \tag{18}$$

The calculated velocity values and their uncertainties are summarized in Table 2.

Tab. 2. Average air velocity values and uncertainties.

Experiment / Noise filtering method	BUB006			BUB004			BUB001		
	υ [m/s]	$u_C(\upsilon)$ [m/s]	$u_{Cr}(\upsilon)$ [%]	υ [m/s]	$u_C(\upsilon)$ [m/s]	$u_{Cr}(\upsilon)$ [%]	υ [m/s]	$u_C(\upsilon)$ [m/s]	$u_{Cr}(\upsilon)$ [%]
IIR filters	0.708	0.012	1.7	1.064	0.021	2.0	1.448	0.035	2.4
$\lvert CSDF \rvert_s$	0.710	0.011	1.6	1.066	0.017	1.6	1.463	0.032	2.2
DWT	0.712	0.010	1.4	1.069	0.015	1.4	1.463	0.023	1.6
NWKE	0.710	0.010	1.4	1.069	0.016	1.5	1.462	0.029	2.0

7. Conclusions

The signals obtained in the two-phase flow measurements using gamma absorption are often characterized by high contribution of disturbances, such as background radiation, fluctuations of nuclear decay, noise of electronic components, etc. This hinders the determination of flow parameters, based on measuring the transportation time delay of signals derived from the scintillation probes.

The paper presents four methods of noise reduction in cross-correlation measurements of the dispersed phase velocity in the liquid-gas mixture flow through a horizontal pipeline. The signals analysed in the article have different signal-to-noise ratios, which provides an opportunity for comparing the effectiveness of the presented methods. In the first analysed solution, the following two noise filtering methods were applied to the signals received from the detectors: classical *IIR* Butterworth filters, and the "spectrum filtration" method. Then the cross-correlation function was determined, and the transportation time delay and the average velocity of the dispersed phase flow were calculated. In the second approach, signal filtration was replaced by smoothing of the cross-correlation function with the discrete wavelet transform or the Nadaraya-Watson kernel estimator.

The signals obtained for three types of flows were analyzed. The lowest velocity uncertainty values were obtained for the plug flow, while the highest for the bubble flow. This is related to the fact that the plug flow is less chaotic than the bubble flow. Hence, the share of noise is the smallest for the former and the largest for the latter flow.

For all types of flows, the lowest uncertainty values were obtained for the discrete wavelet transform, then for the Nadaraya-Watson kernel estimator, "spectrum filtration", and classical *IIR* filtration.

In presented methods of signal analysis, selecting the values of parameters specific to each of them is crucial. The methods which require frequency range determination are based on the signal spectrum. In authors' opinion, in the case of "spectrum filtration", the best results are obtained when analysing the module of smoothed cross-spectral density. For discrete wavelet transformation, the wavelet type and the level of

decomposition should be selected experimentally. Similarly, for Nadaraya-Watson kernel estimator application, the experimentally determined kernel functions and the width of the smoothing window should be selected. In cases of similar results, the suitability of the filtering method should be determined by its simplicity, understood as the minimum number of operations to be performed and the number of parameters to be determined in an experimental way (subjective). Therefore, the authors believe that the most effective methods are *DWT* and *NWKE*. Wherein, due to a smaller number of parameters subjectively matched, the *CCF* approximation using *NWKE* is preferred. In that case, the width of the smoothing window is the most important parameter.

Judging from the effects of the completed investigations, the need for further research of noise reduction methods in radioisotope cross-correlation measurements, including those based on non-parametric regression methods, is evident. In the case of filtration procedures, the search for the selection of straightforward filter parameters aiming to automate noise reduction in industrial measurements is significant.

Funding sources

This publication is funded by AGH University of Science and Technology (No 11.11.140.645) and by Rzeszów University of Technology (U-713/DS).

Conflict of interest

The authors declare that there is no conflict of interests regarding the publication of this paper.

Acknowledgment

The authors would like to thank Dr Alex Wade for his support with writing of the manuscript.

References

[1] G. Falcone, G.F. Hewitt, C. Alimonti, Multiphase flow metering: principles and applications, Elsevier, Amsterdam, 2009.

[2] T.H. Heindela, J.N. Grayb, T.C. Jensenb, An X-ray system for visualizing fluid flows, Flow Meas. Instrum. 19 (2008) 67–78. http://dx.doi.org/10.1016/j.flowmeasinst.2007.09.003.

[3] E. J. Mohamad, et al., Measurement and analysis of water/oil multiphase flow using electrical capacitance tomography sensor, Flow Meas. Instrum. 47 (2016) 62–70. https://doi.org/10.1016/j.flowmeasinst.2015.12.004.

[4] V. Mosorov, Flow pattern tracing for mass flow rate measurement in pneumatic conveying using twin plane electrical capacitance tomography, Part. Part. Syst. Charact. 25 (2008) 259–265. doi:10.1002/ppsc.200700034.

[5] V. Mosorov, Phase spectrum method for time delay estimation using twin-plane electrical capacitance tomography, Electron. Lett. 42 (2006) 630. doi:10.1049/el:20060338.

[6] M. Jaszczur, K. Styszko, J. Tomaszek, K. Zurawska, An analysis of long term temperature measurement using laser induced fluorescence, in: J. Phys. Conf. Ser., 2016. doi:10.1088/1742-6596/745/3/032109.

[7] W.R. de Oliveira, I.B. de Paula, F.J.W.A. Martins, P.S.C. Farias, L.F.A. Azevedo, Bubble characterization in horizontal air–water intermittent flow, Int. J. Multiphas. Flow 69 (2015) 18–30. http://dx.doi.org/10.1016/j.ijmultiphaseflow.2014.10.014.

[8] H.-D. Sommerlatt, A. Andruszkiewicz, Dynamic measurement of particle diameter and drag coefficient using the ultrasonic method, Arch. Acoust. 33 (2008) 351–362.

[9] A. Tamburini, A. Cipollina, G. Micale, A. Brucato, Particle distribution in dilute solid liquid unbaffled tanks via a novel laser sheet and image analysis based technique, Chem. Eng. Sci. 87 (2013) 341–358. http://dx.doi.org/10.1016/j.ces.2012.11.005

[10] T. Xue, L. Qu, Z. Cao, T. Zhang, Three-dimensional feature parameters measurement of bubbles in gas–liquid two-phase flow based on virtual stereo

vision, Flow Meas. Instrum. 27 (2012) 29–36. http://dx.doi.org/10.1016/j.flowmeasinst.2012.07.007.

[11] A. Povolny, H. Kikura, T. Ihara, Ultrasound pulse-echo coupled with a tracking technique for simultaneous measurement of multiple bubbles, Sensors (Switzerland). 18 (2018). doi:10.3390/s18051327.

[12] G.H. Roshani, S.A.H. Feghhi, A. Mahmoudi-Aznaveh, E. Nazemi, A. Adineh-Vand, Precise volume fraction prediction in oil–water–gas multiphase flows by means of gamma-ray attenuation and artificial neural networks using one detector, Measurement 51 (2014) 34-41. https://doi.org/10.1016/j.measurement.2014.01.030.

[13] B.K. Arvoh, R. Hoffmann, M. Halstensen, Estimation of volume fractions and flow regime identification in multiphase flow based on gamma measurements and multivariate calibration, Flow Meas. Instrum. 23 (2012) 56-65. http://dx.doi.org/10.1016/j.flowmeasinst.2011.11.002.

[14] G.H. Roshani, E. Nazemi, S.A.H. Feghhi, S. Setayeshi, Flow regime identification and void fraction prediction in two-phase flows based on gamma ray attenuation, Measurement 62 (2015) 25-32. https://doi.org/10.1016/j.measurement.2014.11.006.

[15] Y. Zhao, B. Qincheng, H. Richa, Recognition and measurement in the flow pattern and void fraction of gas-liquid two-phase flow in vertical upward pipes using the gamma densitometer, Appl. Therm. Eng. 60 (2013) 398-410. http://dx.doi.org/10.1016/j.applthermaleng.2013.07.006.

[16] M. Zych, R. Hanus, L. Petryka, Application of spectral analysis in radiometric measurements of two-phase liquid-gas flow, MATEC Web Conf. 18 (2014) 02004. http://dx.doi.org/10.1051/matecconf/20141802004.

[17] M. Zych, R. Hanus, L. Petryka, A. Strzępowicz, P. Zych, W. Mastej, Selected noise reduction methods in correlation two-phase flows measurements by radioisotopes, Przegl. Elektrotech. 90(8) (2015) 66-68. (in Polish) 10.15199/48.2015.08.17.

[18] M.S. Beck, A. Pląskowski, Cross-correlation flowmeters. Their design and application, Adam Hilger, Bristol, 1987.

[19] J.S. Bendat, A.G. Piersol, Random data. Analysis and measurement procedures, fourth ed., John Wiley, New York, 2010.

[20] R. Hanus, M. Zych, L. Petryka, Velocity measurement of the liquid–solid flow in a vertical pipeline using gamma-ray absorption and weighted cross-correlation, Flow Meas. Instrum. 40 (2014) 58–63. http://dx.doi.org/10.1016/j.flowmeasinst.2014.08.007.

[21] R. Hanus, M. Zych, A. Kowalczyk, L. Petryka, Velocity measurements of the liquid - gas flow using gamma absorption and modified conditional averaging, EPJ WoC 92 (2015) 02021. http://dx.doi.org/10.1051/epjconf/20159202021.

[22] R. Hanus, Application of the Hilbert Transform to measurements of liquid-gas flow using gamma ray densitometry, Int. J. Multiphas. Flow 72 (2015) 210-217. http://dx.doi.org/10.1016/j.ijmultiphaseflow.2015.02.002.

[23] M. Zych, R. Hanus, L. Petryka, D. Świsulski, A. Strzępowicz, P. Zych, Application of gamma densitometry and statistical signal analysis to gas phase velocity measurements in pipeline hydrotransport, EPJ WoC 92 (2015) 02122. http://dx.doi.org/10.1051/epjconf/20159202122.

[24] G.F. Knoll, Radiation detection and measurement, third ed., John Wiley & Sons, Inc., New York, 2000.

[25] P. Augustyniak, Time-frequency modelling and discrimination of noise in the electrocardiogram, Physiol. Meas. 24 (3) (2003) 753–767. iopscience.iop.org/article/10.1088/0967-3334/24/3/311.

[26] B. Buttkus, Spectral analysis and filter theory in applied geophysics, Springer-Verlag, Berlin, 2000.

[27] J. Jarzyna, M. Bała, P. Krakowska, Multi-method approach to velocity determination from acoustic well logging, Ann. Soc. Geol. Poloniae 83 (2013) 133–147. https://geojournals.pgi.gov.pl/asgp/article/view/12596/11069.

[28] K. Wawrzyniak, Application of time-frequency transforms to processing of full waveforms from acoustic logs, Acta Geophys. 58 (2010) 49–82. https://link.springer.com/article/10.2478/s11600-009-0043-4.

[29] M. Habrat, P. Krakowska, E. Puskarczyk, M. Jędrychowski, P. Madejski, Technical Note. the Concept of a Computer System for Interpretation of Tight Rocks Using X-Ray Computed Tomography Results, Stud. Geotech. Mech. 39 (2017) 101–107. doi:10.1515/sgem-2017-0010.

[30] M. Łój, S. Porzucek, An example of subsurface microgravimetry survey, in: 15th Int. Multidiscip. Sci. GeoConference SGEM 2015, B. 1, 2015: p. 743–752 pp. doi:10.5593/SGEM2015/B11/S4.095.

[31] M. Zych, R. Hanus, K. Kozak, T. Zorski, V. Mosorov, J. Mazur, L. Petryka, P. Zych, A. Strzępowicz, Comparison of methods for noise reduction of gamma energy spectra, XXI IMEKO World Congress “Measurement in Research and Industry” Aug. 30 – Sept. 4, 2015, Prague, Czech Republic, Full Papers Book, 1835-1839.

[32] S. Efromovich, Nonparametric Curve, methods, theory, and applications, Springer-Verlag Inc., New York, 1999.

[33] T. Hastie, R. Tibshirani, J. Friedman, The elements of statistical learning. Data mining, inference, and prediction, second ed. Springer Science + Business Media, New York, 2009.

[34] M.L.S. Indrusiak, S.V. Möller, Wavelet analysis of unsteady flows: Application on the determination of the Strouhal number of the transient wake behind a single cylinder, Exp. Therm. Fluid Sci. 35 (2011) 319–327. http://dx.doi.org/10.1016/j.expthermflusci.2010.10.001.

[35] S. Mallat, A wavelet tour of signal processing, Academic Press, third ed. Burlington, 2009.

[36] J.-L. Starck, F. Murtagh, J.M. Fadilli, Sparse image and signal processing. Wavelets, curvelets, morphological diversity, Cambridge University Press, New York, 2010.

[37] T. Burr, M. Hamada, N. Hengartner, Impact of spectral smoothing on gamma radiation portal alarm probabilities, Appl. Radiat. Isot. 69 (2011) 1436-1446. http://dx.doi.org/10.1016/j.apradiso.2011.05.009.

[38] J.-J. González-de-la-Rosa, A. Agüera-Pérez, J.-C. Palomares-Salas, J.M. Sierra-Fernández, Wavelets' filters and higher-order frequency analysis of acoustic emission signals from termite activity, Measurement 93 (2016) 315-318. http://dx.doi.org/10.1016/j.measurement.2016.07.037.

[39] F. de Asís López, C. Ordóñez, J. Roca-Pardiñas, S. García-Cortés, Point cloud comparison under uncertainty. Application to beam bridge measurement with terrestrial laser scanning, Measurement 51 (2014) 259-264. http://dx.doi.org/10.1016/j.measurement.2014.02.013.

[40] Guide, 1995. Guide to the expression of uncertainly in measurement. International Organization for Standardization.

Marcin Zych, received his Ph.D. in Applied Physics in 2007. He is working at the AGH-University of Science and Technology in Krakow, Faculty of Geology, Geophysics and Environment Protection. Scientific interests include: application of radioisotopes in geophysics (particularly well logging) and industrial processes, signal analysis and radiology protection.

Robert Hanus, received his Ph.D. and tenured at the Lviv Polytechnic National University (Ukraine) in 1997 and Rzeszow University of Technology (RUT, Poland) in 2016, respectively. He is currently employed as an associate professor in the RUT Department of Metrology and Diagnostic Systems, where his interests are in signal processing and measurement systems. His publications can be found at www.researchgate.net and http://scholar.google.pl

Barbara Wilk, received the Ph.D. degree in electronics from Wrocław University of Science and Technology. She is working at the Rzeszow University of Technology, Department of Metrology and Diagnostic Systems. Her major research interests include digital signal processing of biomedical signals.

Leszek Petryka, received M.S., Ph.D. and tenured successively at the AGH University of Science and Technology. He has exclusively focused on Applied Physics, particularly two-phase flows and radioisotope applications. He has arranged a number of industrial experiments and was the IAEA Expert to Indonesia and Malaysia. His publications may be found at www.researchgate.net and http://scholar.google.pl.

Dariusz Świsulski, received his Ph.D. degree and tenured at the Gdansk University of Technology in 1995 and 2006. He is currently employed as the Head of Department of Control System Engineering at the Faculty of Electrical and Control Engineering at Gdansk University of Technology. He is interested in the fields of: metrology, measurement systems and signal processing.